Acta Astronautica 249 (2026) 217–227

Contents lists available at ScienceDirect

Acta Astronautica

journal homepage: www.elsevier.com/locate/actaastro

Sea-island microstructure and spontaneous confinement layer formation in polyamide 6/polybutylene terephthalate films for improved laser propulsion efficiency

P. Battocchio [a,*,1], D. Di Liberto [b,1], G. Fredi [b], A. Pegoretti [b], A. Miotello [a]

[a] Department of Physics, University of Trento, Via Sommarive 14, Trento, 38123, Italy
[b] Department of Industrial Engineering and INSTM Research Unit, University of Trento, Via Sommarive 9, Trento, 38123, Italy

ARTICLE INFO

Keywords:
Laser ablation propulsion
Nano-satellites propulsion
Confined laser ablation
Immiscible polymer blends
Laser thermal decomposition

ABSTRACT

Laser ablation propulsion (LAP) represents a promising approach for nano-satellite propulsion, owing to its high exhaust velocity and the possibility of remote thrust generation. Polymeric materials are particularly attractive as LAP targets due to their low ablation thresholds and possible high laser impulse coupling coefficients. In this study, polymeric films based on immiscible blends of polyamide 6 (PA6) and polybutylene terephthalate (PBT) are investigated with the aim of enhancing impulse generation through confined laser ablation. The intrinsic immiscibility of PA6 and PBT gives rise to a sea-island microstructure which is exploited to promote the spontaneous formation of a confinement layer during laser irradiation. The blend morphology and optical absorption properties were characterized by scanning electron microscopy and UV-Vis spectroscopy, respectively, while impulse generation under vacuum conditions was quantified using a custom ballistic pendulum. By tuning the PBT concentration, an optimal composition was identified at which the onset of confined ablation coincides with surface layer detachment and a maximum in the generated impulse. These results demonstrate that the sea-island microstructure plays a critical role in enabling spontaneous confinement effects, offering a viable strategy for the design of advanced polymeric targets for laser ablation propulsion.

1. Introduction

The New Space Economy is making space environment accessible to several organizations, driving a surge in nano-satellite launches and enabling full Earth coverage and rapid data updates through satellite constellations [1]. This was made possible by the advent of microelectronics, leading to the possibility of manufacturing lighter nano-satellites, e.g., CubeSats, allowing a *democratization of space* [2]. In the meantime, the small size of these devices demands new propulsion systems for orbit correction, preferably not included in the satellite itself for mass and size limitations. In contrast, this phenomenon is leading to progressive Earth orbital congestion, causing collisions between satellites and leading to a severe increment of space debris [3].

Laser ablation propulsion (LAP) is gaining interest thanks to its advantages with respect to conventional propulsion techniques, relying on the possibility to propel objects far from the laser source thanks to the high ejection velocity of ablated products that generate thrust in the opposite direction on the target, because of momentum conservation [4]. The impulse generated by the laser hitting the target is therefore defined as:

$$J = m_e v_e \ [\mu\text{N s}] \tag{1}$$

where m_e is the ejected mass while v_e is the exhaust velocity. While in the case of space debris mitigation it is not possible to optimize the target material, the choice of the most suitable material in nano-satellite propulsion is of paramount importance. Laser-impulse coupling coefficient (C_m), is one of the main parameters to be considered in the choice of a material for a specific mission. It is defined as in Equation (2):

$$C_\text{m} = \frac{\text{generated impulse}}{\text{laser energy}} = \frac{J}{E}\left[\frac{\mu\text{N s}}{\text{J}}\right] \tag{2}$$

C_m describes the amount of laser energy a material requires to generate a given mechanical impulse, and it is a function of laser fluence. Along

* Corresponding author.
E-mail address: pietro.battocchio@unitn.it (P. Battocchio).
[1] These two authors contributed equally.

https://doi.org/10.1016/j.actaastro.2026.08.047
Received 18 May 2026; Received in revised form 7 August 2026; Accepted 17 August 2026
Available online 19 August 2026

with C_m, the propulsion performance can also be described in terms of specific impulse (I_{sp}), defined as:

$$I_{sp} = \frac{J}{m_e g_0} = \frac{v_e}{g_0} \; [s] \tag{3}$$

With g_0 the gravity acceleration on Earth. I_{sp} relates the generated impulse with the amount of ejected mass, and indicates its ejection velocity during ablation. Finally, a third parameter that allows to describe the impulse generation process is its energetic efficiency (η), that is defined as the ratio of the kinetic energy of the ejected mass to the laser energy. It can be written as:

$$\eta = \frac{1}{2} C_m I_{sp} g_0 \tag{4}$$

In nano-satellite propulsion, polymers emerge as good candidates rather than metals, due to their higher values of C_m, thanks to their lower ablation threshold [5]. Among the most widely used polymers, polyoxymethylene (POM) [6,7], polytetrafluoroethylene (PTFE) [8], polyvinylchloride (PVC) [9,10], and glycidyl azide polymer (GAP) [11] have been studied for the application. Additionally, different strategies have been studied to increase the laser impulse coupling coefficient, such as including laser absorbers like carbon nanoparticles in polymeric matrices [9]. This strategy has also been extended by including metallic nanoparticles in polymers [12] or by reinforcing the polymer matrix with a metallic mesh [13]. In all these cases, the goal was to enhance the optical interaction of a polymer matrix with the laser by including localized absorbers, a procedure that proved to be effective in improving plasma expansion and thrust generation. Among the alternatives, either multilayer structures [10,14] or materials capable of delivering spontaneous confinement effects have been explored [15], inducing confinement effects in the ablation process to increase the generated impulse.

In both cases, the impulse enhancement is obtained by the presence of a transparent material initially blocking the expansion of the plasma produced during ablation, and thus favoring pressure increase until the transparent layer is violently expelled [16]. This effect was largely studied in the case of metals [16–19], but it still requires study in the case of polymers.

In our previous work [15], we observed the spontaneous formation of a confinement layer during the irradiation of a nanocomposite material containing poly (lactic acid) (PLA), poly(1,12- dodecamethylene 2,5-furandicarboxylate) (PDoF), and reduced graphene oxide (rGO) as filler. In that case, the formation of the confinement layer was attributed to the formation of a sea-island microstructure in which a transparent PLA matrix surrounds volumes of PDoF + rGO that strongly absorb the laser radiation. However, the generalization of the suggested mechanism to other materials with a similar structure and different fabrication procedures was still lacking, along with a more detailed description of the role of the thickness of the matrix, which in the case of [15] could not be modified. Additionally, the role of strongly absorbing rGO filler in the process was still not well defined, since its absence prevented completely the formation of the confinement layer.

The goal of this work was therefore to reproduce a sea-island microstructure with similar optical properties while avoiding the use of carbonaceous fillers, to prove that the spontaneous formation of a confinement layer can also be reproduced by exploiting intrinsic properties of immiscible polymer blends. To this aim, polyamide 6 (PA6) was chosen as the matrix, due to its low absorption to the laser wavelength used here, while polybutylene terephthalate (PBT) was chosen as a strongly absorbing phase. The choice of this pair of polymers was also driven by their immiscibility, which led to the formation of the desired sea-island structure. The composition of the blend was also changed in order to investigate how the thickness of the transparent matrix affected the mass ejection process. Additionally, the synthesis of the samples was performed through melt compounding and hot pressing, as a possible scalable technique to obtain larger films. The microstructure of the prepared samples was examined using scanning electron microscopy (SEM), while optical absorption was analyzed via UV-Vis spectroscopy. A custom ballistic pendulum system allowed the measurement of impulse generation under vacuum laser ablation, and of the ablated mass [20]. Subsequently, the propulsion parameters C_m, I_{sp} and η were evaluated for a comprehensive propulsion analysis of the system, and the ablation mechanism was discussed thoroughly.

2. Methods

2.1. Materials

Polyamide 6 (PA6) Radilon® S24 100 NT granules were supplied by Radici Group s. p.a. (Gandino, Bergamo, Italy). A melting point of 223 °C and a glass transition at around 53 °C were measured by differential scanning calorimetry (DSC). Polybutylene terephthalate (PBT) Pocan® B110 was provided by Lanxess s. r.l. (Segrate, Milano, Italy) in the form of pellets. It shows measured (by DSC) glass transition temperature of 43 °C and melting temperature of 225 °C. These specific materials were chosen for the application due to their immiscibility, to their similar melting points, granting easy processability through melt compounding, and due to their differences in optical absorption, which were evaluated through the analyses described in Paragraph 2.3.

2.2. Preparation of blend films

The blends were prepared via melt compounding in controlled conditions in a Thermo Haake® Rheomex internal mixer at 230 °C for 10 min at 60 rpm to ensure proper mixing. Materials were pre-dried overnight in vacuum conditions at 80 °C to reduce moisture content. After blending, the compounded materials were hot-pressed in a Carver laboratory press, applying 7 tons for 5 min. In the end, films with thicknesses ranging from 50 to 100 μm were obtained. All the prepared nominal compositions are reported in Table 1.

2.3. UV-visible spectroscopy

UV-Visible spectroscopy was utilized to measure the laser absorbance of the polymeric films and the absorption coefficients of the single components, which were evaluated according to the Lambert-Beer law:

$$I(h) = I_0 \exp(-\alpha h) \tag{5}$$

Where I_0 and $I(h)$ are respectively the incoming and the transmitted intensity, h is the length of the optical path and α is the absorption coefficient. This analysis allows the assessment of the effect given by adding PBT to the optical properties of PA6. The measurements were carried out at the used laser wavelength of 266 nm, using a Varian Cary 5000 spectrophotometer.

2.4. Microstructural analysis

The cross-section morphology of the polymeric films was analyzed via a Carl Zeiss® Supra field emission scanning electron microscopy

Table 1
Nominal compositions of prepared blends.

Sample	PA6 [wt%]	PBT [wt%]
PA6	100	0
PA6:PBT (99:1)	99	1
PA6:PBT (98:2)	98	2
PA6:PBT (95:5)	95	5
PA6:PBT (80:20)	80	20
PA6:PBT (60:40)	60	40
PBT	0	100

(FESEM). Samples were fractured in liquid nitrogen to ensure a fragile fracture and to promote the formation of a flat fracture surface. The analyzed surfaces were covered with a Pt/Pd layer to make them electrically conductive. This analysis was performed to observe the miscibility between the two polymers and to correlate this information with impulse measurements. Image analysis was also performed on the acquired cross-sections by using ImageJ to estimate the average size of PBT domains and their relative distances. Additionally, FESEM was used to analyze the morphology of the surface of the ablated craters, to assess the effects of the materials-laser interaction after the ablation process.

2.5. Impulse measurement

The impulse produced during ablation was quantified using the experimental setup and data analysis procedure described in detail in Ref. [20], for laser fluences ranging from 0 to 7 J cm^{-2}. Laser fluence was selected both by changing laser pulse energy, as measured by an energy meter, and by varying the laser spot and changing the distance from the target of a lens with a 200 mm focal length. To cover this fluence range, two different laser spot areas ($A_{irradiated}$) of 3.7± 0.1 mm^2 and 1.0 ± 0.1 mm^2 were used, measured through the analysis of optical microscope images of the ablation craters. To account for differences in the magnitude of the ablated area, impulse per unit area was considered, allowing to obtain coherent impulse curves as a function of laser fluence. The experimental apparatus is depicted in Fig. 1.

The measurement method relies on detecting the change in angular momentum of a ballistic pendulum, induced by the mechanical impulse imparted upon it. The fourth harmonic of a Nd:YAG laser (Litron TRLi-G 850-10), emitting at a wavelength of 266 nm with a pulse duration of 5 ns, was used for the measurements. The pendulum oscillates before and after the impulse event, with typical amplitudes of less than 1°. To accurately track these oscillations, a probe laser is directed at a mirror mounted on the top of the pendulum. The motion of the reflected probe beam across a graduated scale is recorded using a high-speed camera operating at 1000 frames per second. This setup effectively creates a long optical arm, which enhances the detection of small angular displacements.

By analyzing the pendulum motion as a function of time, both before and after the application of the impulse, it is possible to determine the exact moment at which the impulse occurs. From this, the resulting change in angular velocity ($\Delta\omega$) can be calculated. Given that the impulse acts orthogonally to both the target surface and the pendulum rotational axis, the change in angular momentum can be expressed as:

$$J = \frac{I\Delta\omega}{r} \tag{6}$$

Here, J represents the mechanical impulse, I the moment of inertia of the pendulum, and r the radial distance from the axis of rotation of the pendulum to the center of the irradiated spot where the force is applied. Both r and I are determined through image analysis, as outlined in Ref. [10].

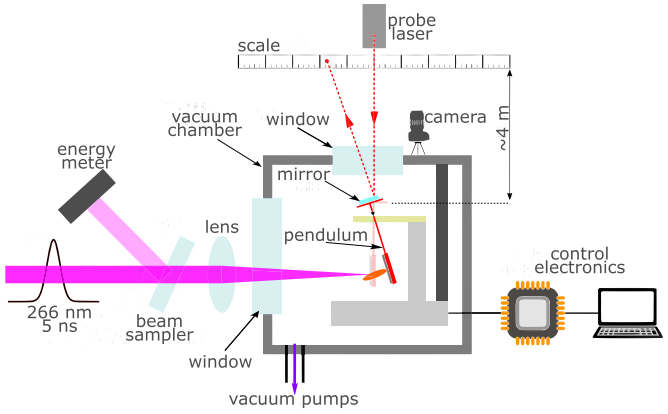

Fig. 1. Scheme of the experimental apparatus used for impulse measurements.

A significant advantage of using a ballistic pendulum for impulse measurements is that it does not require calibration of the apparatus, thereby eliminating potential calibration-related errors. As detailed in Ref. [10], the experimental uncertainties are assessed by estimating and propagating individual error sources throughout each stage of the analysis. Due to the reduced thickness of the prepared polymeric films, the samples were fixed with double-sided tape on a laboratory glass slide acting as a support, which in turn was fixed to the ballistic pendulum. All measurements were conducted under high vacuum conditions, with pressures maintained below 10^{-4} mbar. To ensure consistent experimental conditions and uniformity of the target material, the ablated region on the polymer surface was shifted after each laser pulse, thus avoiding multiple exposures of the same area, except during multiple-irradiation measurements.

2.6. Ablated mass measurement

To measure the ablated mass, thin film specimens were weighed before and after irradiation through multiple pulses. To avoid any variation in the environment with respect to impulse measurements, the samples were fixed on the same ballistic pendulum as previously described. For each laser fluence selected, a certain number of shots (n_{shots}) ranging from 40 to 120 was used, depending on the irradiation area. A new region was irradiated at each shot, exactly as for impulse measurements, with the difference that in this case the pendulum was held stationary. The ablated mass per unit area (Δm) was estimated for each composition, at each fluence as:

$$\Delta m = \frac{m_i - m_f}{n_{shots}\, A_{irradiated}} \tag{7}$$

where m_i is the mass before irradiation, m_f is the mass afterwards, both measured by means of a balance with 10^{-5} g resolution. Equation (7) allows to compare the results of Δm based on the different laser fluences, which are obtained by changing laser pulse energy and $A_{irradiated}$. Errors in the measurements are related to the balance resolution and to the actual crater areas.

3. Results and discussion

3.1. UV-visible spectroscopy

UV spectroscopy measurements provide information on the optical interaction between PA6 and PBT with the laser. From the measurements, it emerges that, at the investigated laser wavelength, PA6 is more transparent than PBT. This was confirmed by the measurement of the absorption coefficients, namely α_{PA6} of 553 cm^{-1} and α_{PBT} of 3448 cm^{-1}. Due to these differences, it is expected that when irradiated, PA6 partially allows the transmission of radiation, while a large part of the radiation is absorbed by PBT, so that its ablation process is expected to occur in much shorter times, due to the higher heating rate.

3.2. Cross-section microstructure

SEM images of the cryo-fractured cross-section of the prepared films before irradiation are reported in Fig. 2(a–e). The microstructure portrayed by all compositions has a sea-island morphology, typical of immiscible blends. Notably, in all the samples, spherical domains of PBT appeared uniformly dispersed in PA6. Analysis of the SEM images of the cross-section shows that, by increasing the amount of PBT, domains become larger and closer to each other, as presented in Fig. 2(f). This contributes to increasing the number density of laser absorption sites and of the interfaces between PA6 and PBT, where the laser is expected

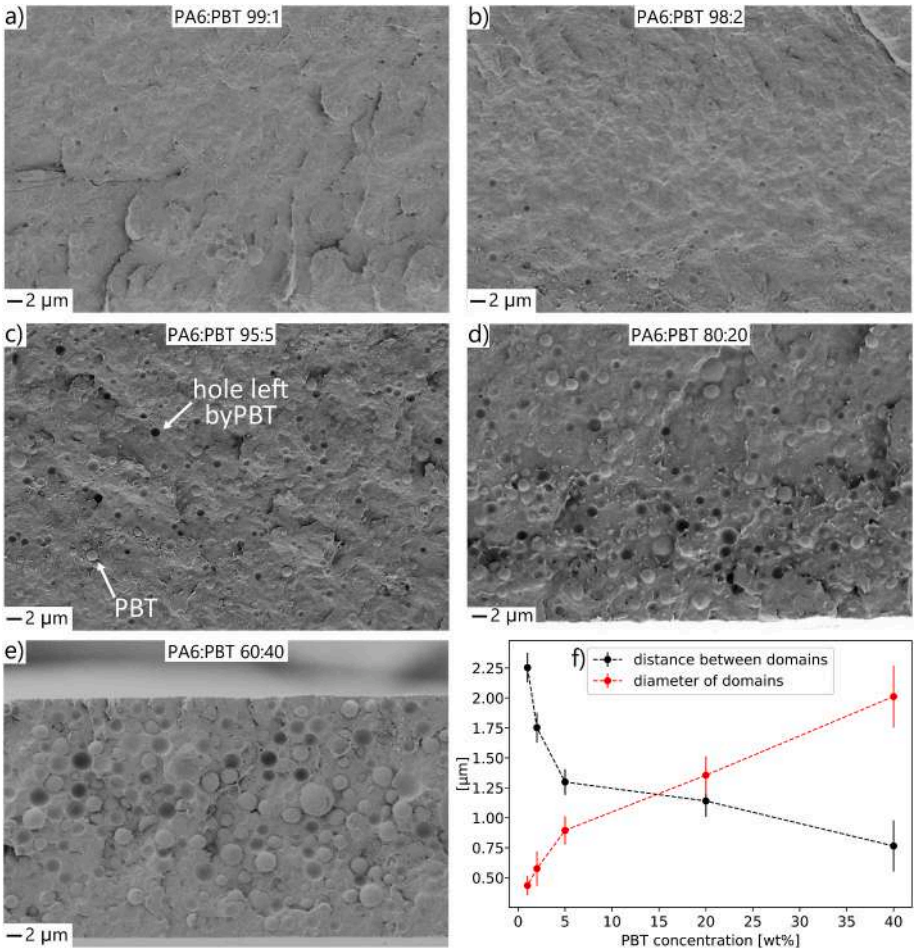

Fig. 2. SEM images of the cross-section of the prepared films with increasing amount of PBT. a) 1 wt%, b) 2 wt%, c) 5 wt%, d) 20 wt%, e) 40 wt%. f) Plot of the average diameters of PBT domains according to the blend composition, and distance among them, obtained from image analysis. Uncertainties are estimated by propagation of the error in the calibration lengths in the image and of the standard variation of the radii of the PBT volumes.

to be absorbed. At the same time, a reduced distance between PBT domains indicates a thinner PA6 matrix surrounding them.

The observed microstructure of the prepared materials is similar to the one presented in Ref. [15], where the formation of a confinement layer was obtained during laser irradiation. In that work, the ratio between the two mixed polymers was fixed, and the observed behavior was a function of the amount of the filler, which was present either only inside spherical domains or also inside the matrix. In this case, no filler is present, while the ratio between the two polymers is changed.

3.3. Impulse measurement

Fig. 3(a) shows the impulse generated after irradiation of some different compositions of the PA6:PBT blends, as a function of the laser fluence. In the case of PA6, no impulse is measured for fluences below $\sim$ 3 J cm^{-2}, due to its low laser absorption, while with PBT concentrations as low as 1 wt%, an increase in impulse generation can be observed. In this low concentration range, all impulse curves show a similar shape, and impulse increases with PBT content because of a reduction in the fluence threshold for impulse generation(F_{th}). This is well visible in Fig. 3(b), presenting the values of F_{th} estimated by performing a linear fit on the initial increasing part of impulse curves. The decreasing trend of F_{th} with PBT concentration shows that when the number density of absorbers increases, absorbed laser energy is used more efficiently to reach ablation [9].

With a further increase in PBT concentration, a different behavior in the impulse curves can be observed, as depicted in Fig. 3(a), showing an abrupt increase in the impulse at the minimum fluence. As it is also confirmed from Fig. 3(b), in this higher concentration range, starting from PA6:PBT 80:20, no further decrease in F_{th} is observed, indicating that, below this limiting fluence, laser energy becomes too low even to reach a temperature increase able to promote evident ablation processes of PBT. An analogous mechanism was described in Ref. [9].

An interesting aspect emerges when comparing the mechanical impulse behavior, as a function of laser fluence, for various PA6:PBT ratios. The impulse value of neat PBT always prevails up to approximately F $=$ 2 J cm^{-2}, after which it is exceeded by targets with mixed PA6:PBT compositions.

This behavior is well summarized by Fig. 3(c), which shows impulse measured at fixed fluence values as a function of PBT concentration. For fluences lower than 2 J cm^{-2}, the generated impulse grows with PBT concentration, reaching a constant value. In the case of higher fluences, it can be observed that the impulse rapidly increases with PBT concentration, reaching a maximum at 5 wt% of PBT. This result indicates the existence of an optimal PBT concentration for which the impulse is maximized, suggesting that the material's microstructure and composition ratios play a role in the impulse generation process. More generally, by comparing these results with the cross-section images in Fig. 2, it is possible to assess that the number density of PBT volumes and the thickness of the PA6 matrix surrounding them affect the ablation mechanism and the mass ejection process.

C_m curves are presented in Fig. 4. The low values of F_{th} observed in case of high PBT concentration lead to a maximum C_m value at fluences lower than 1 J cm^{-2}, as visible in the case of neat PBT and PA6:PBT

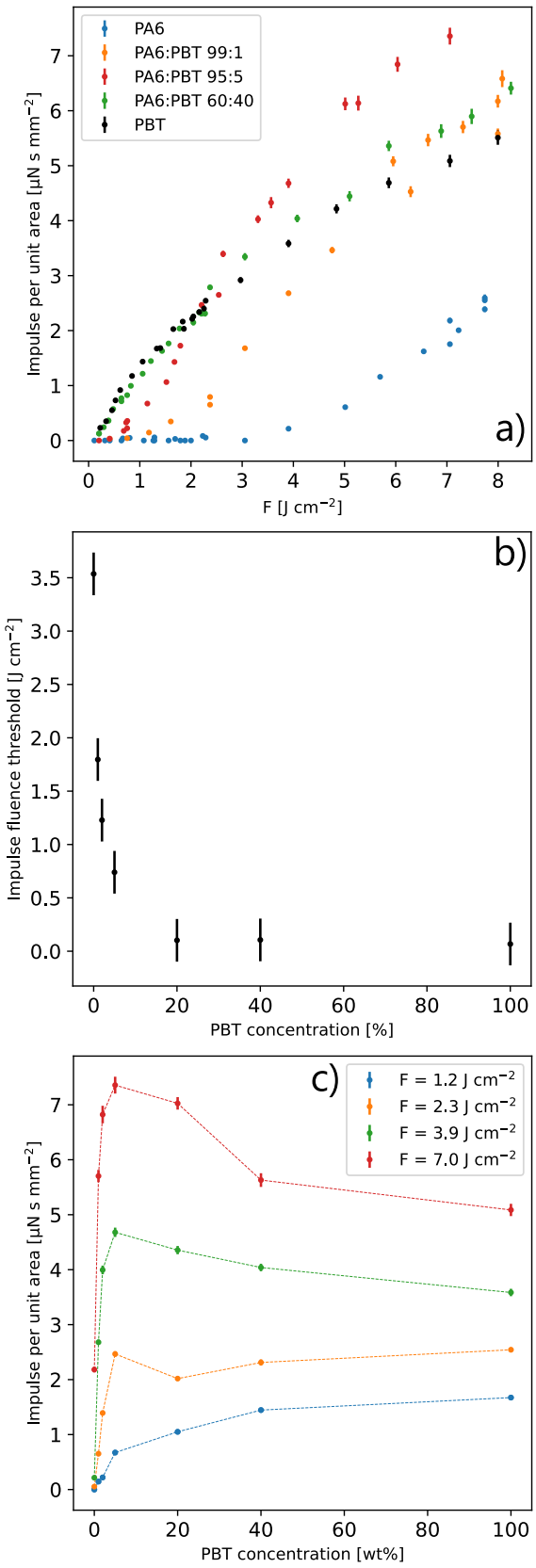

Fig. 3. a) Impulse measurements on the PA6:PBT samples. Impulse curves corresponding to PA6:PBT 98:2 and PA6:PBT 80:20 are not shown for clarity. b) Fluence threshold for impulse generation as a function of PBT concentration. c) Generated impulse at fixed fluence as a function of PBT concentration. Non-visible error bars are smaller than the marker.

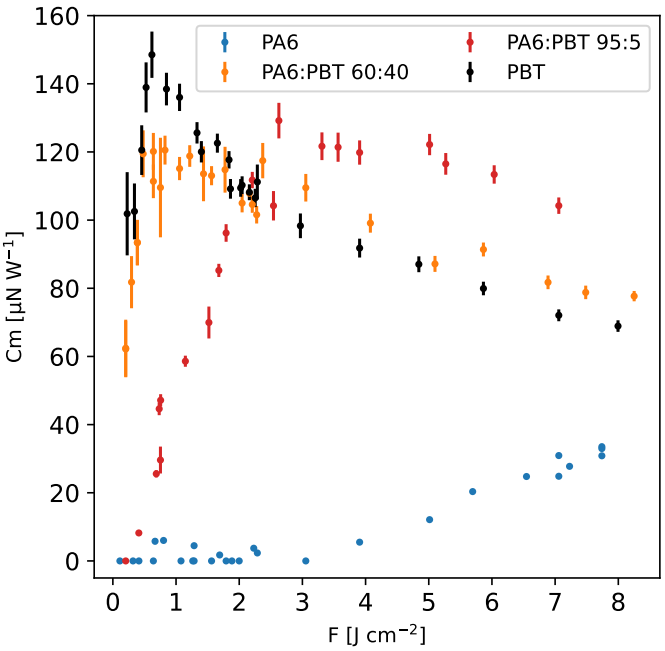

Fig. 4. C_m curves for some of the samples investigated. Non-visible error bars are smaller than the marker.

60:40. Reducing PBT concentration, maximum C_m value slightly decreases and moves to higher fluence, as observed in case of PA6:PBT 95:5. The higher impulse obtained for PA6:PBT 95:5 for $F > 2$ J cm^{-2} also leads to higher C_m values in this fluence range when compared to other concentrations. This shows that impulse generation at this composition requires a lower amount of energy, making the process more efficient from this point of view, compared to neat PBT and PA6. Overall maximum C_m values are a bit lower if compared to the ones measured in the previous work of our group. However, these values result to be superior to other more conventional systems previously studied [8,10,15,21].

In order to test the effect of multiple irradiations on the same region, further impulse measurements were performed on the sample PA6:PBT 95:5, since here it allows the best results for laser propulsion. Each region was irradiated three times without moving the target, and the generated impulse was measured for each laser shot. Each measurement was performed 3 min after the previous one, to avoid a large temperature increase on the crater because of the previous irradiation.

As presented in Fig. 5, impulse generation by PA6:PBT 95:5 slightly decreases after the first pulse, particularly at higher laser fluence. On the other hand, no difference in impulse generation is observed between the second and third pulse. Despite the decrease observed after the first shot (typically <15% for all tested laser fluences), impulse generated by PA6:PBT 95:5 remains higher than that generated by neat PBT, at fluences higher than 2 J cm^{-2}. Such a limited decrease in impulse generation by successive pulses indicates that the interaction of the material with laser radiation is only slightly affected by the previous mass removal process. This suggests that only the PBT domains closer to the surface are removed by the ablation process, while the ones located deeper in the film's thickness are not affected and remain surrounded by the PA6 matrix. Such behavior allows an impulse enhancement given by confinement, also by irradiating the same region multiple times, differently from what occurs in a classical confinement geometry. This observation shows that the improved impulse generation induced by the sea-island microstructure makes this category of materials effective as propellants for nanosatellite propulsion, even by undergoing multiple laser irradiations.

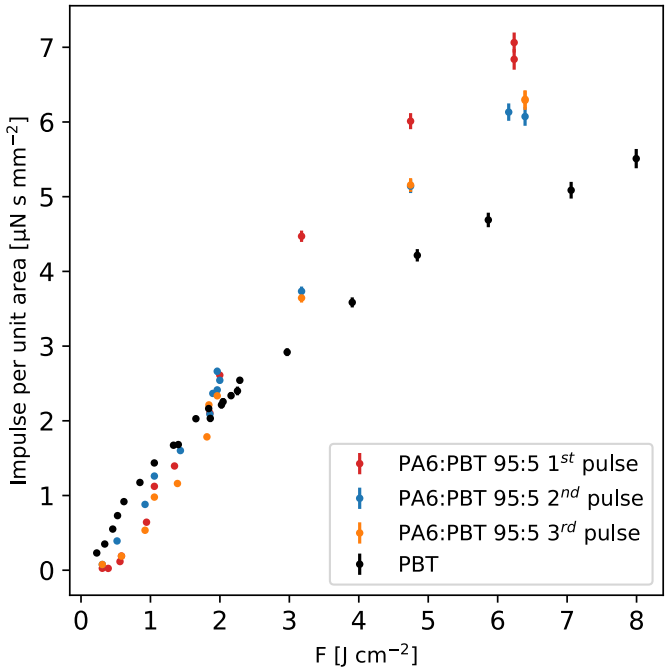

Fig. 5. Impulse generation by PA6:PBT 95:5 for consecutive laser pulses on the same region. Impulse curve for PBT is added as reference. Where not visible, error bars are smaller than the marker.

3.4. Ablated mass measurement

Fig. 6 presents ablated mass measurements at constant fluences as a function of PBT concentration. As previously observed for impulse measurements in Fig. 3(c), also in the case of ablated mass, a maximum is observable at 5 wt% PBT content for all considered fluences.

The trend of the ablated mass as a function of PBT content gives some indications about the interaction of the material with the laser radiation. Ablated mass increases with PBT content up to 5 wt% because PBT absorbs the laser wavelength more effectively than the PA6 matrix. At these concentrations, PBT facilitates energy capture and heat generation, promoting decomposition and a pressure buildup that boosts ablation efficiency across the entire blend, compared to the neat components.

Above 5 wt% of PBT, however, mass loss decreases due to a denser PBT decomposition plume that screens the laser energy. The higher mass loss at 7 J cm^{-2} likely stems from plasma-surface coupling, which improves thermal energy transfer to the substrate.

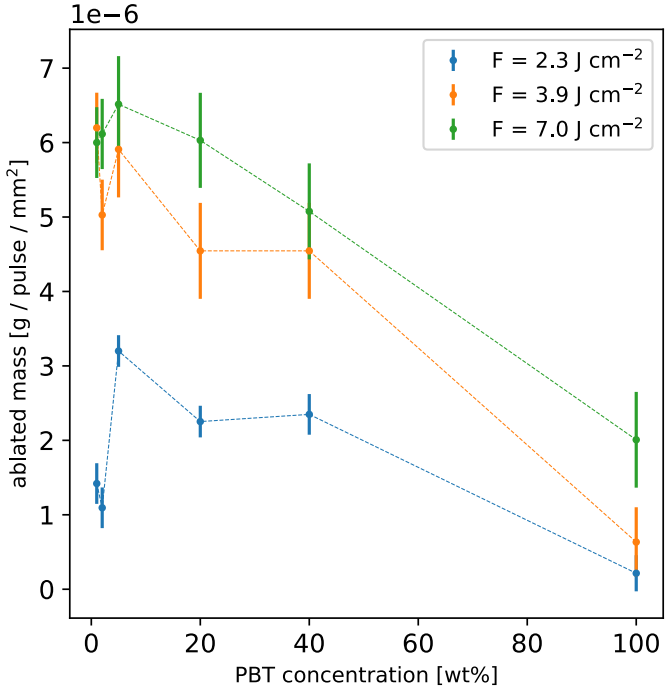

Fig. 6. Ablated mass measurements as a function of PBT concentration.

3.5. Specific impulse and energetic efficiency

Specific impulse obtained on the blends is reported in Fig. 7(a) as a function of PBT concentration, while values for neat PBT are listed in Table (2). At all considered laser fluences and for PBT content higher

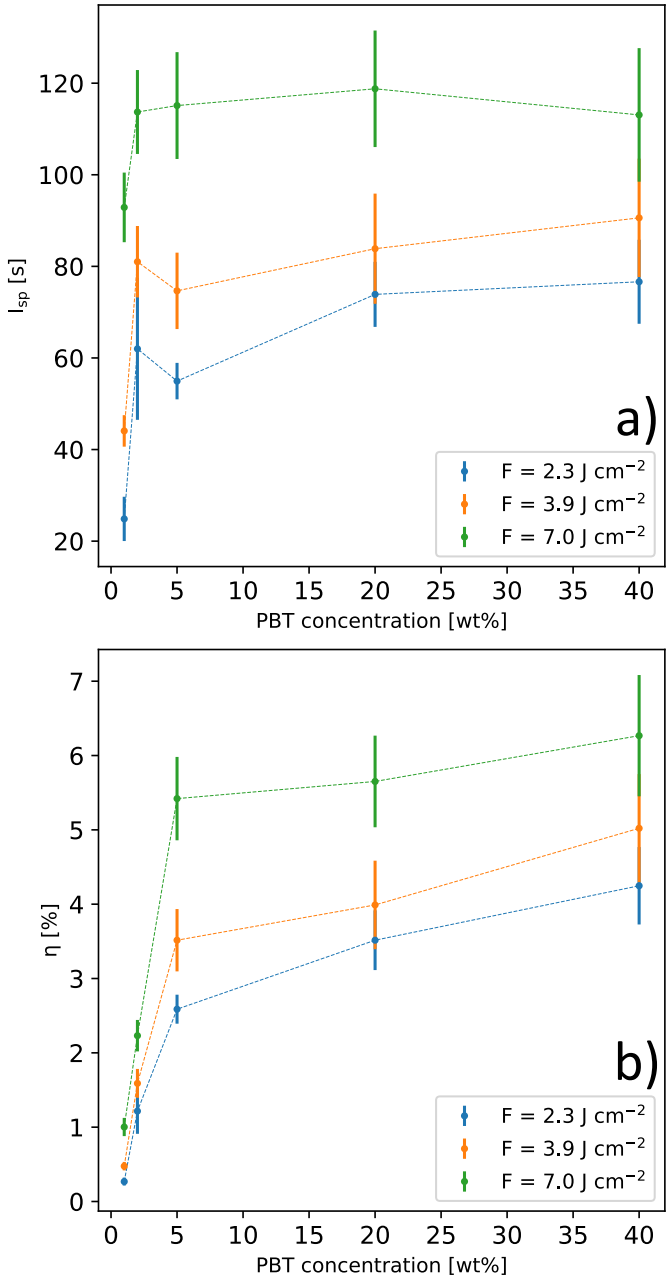

Fig. 7. a) Specific impulse (I_{sp}) and b) energetic efficiency (η) as a function of PBT concentration. Uncertainties are obtained through propagation of the errors of the involved parameters.

Table 2
I_{sp} and η for neat PBT.

Fluence [J cm^{-2}]	I_{sp} [s]	η [%]
2.3	1200 ± 700	70 ± 30
3.9	600 ± 200	30 ± 12
7.0	260 ± 40	14 ± 5

than 1 wt%, I_{sp} reaches a constant value, indicating a constant average ejection velocity of the ablation products. This suggests a similar mechanism of acceleration of the ejected products within the investigated concentration range, indicating that impulse generation is controlled by the amount of the ablated mass. For 1 wt% PBT concentration, a lower I_{sp} is observed, indicating that the removed mass is ejected with a lower velocity, due to the limited portion of mixed polymers absorbing laser radiation and the larger amount of energy required to break the thicker PA6 matrix.

For all the compositions of the blend, I_{sp} is also observed to increase with laser fluence. The increase of the generated impulse with fluence observed in Fig. 3(c) is therefore also related to the increased velocity of the ejected mass.

As can be observed from Fig. 7(b), energetic efficiency η shows a behaviour similar to I_{sp}. This is expected, since η shows the amount of laser energy converted into kinetic energy of the ejected ablated mass, and is therefore strongly dependent on the ejection velocity. However, while for I_{sp} an approximately constant value is reached already at 2 wt % PBT content, in the case of η an almost constant behavior is reached at 5 wt%. The lower increase of η compared to I_{sp} at low concentrations is then reasonably due to the lower amount of ejected mass, which reduces C_m at the considered fluences.

As presented in Table (2), I_{sp} and η obtained for neat PBT are considerably higher than the values obtained in the PA6:PBT blend. Large errors in these measurements are due to the propagation of the large relative error on the small ablated mass observed for PBT. Despite this, it can be observed that both I_{sp} and η decrease with laser fluence. This effect can be related to a different mass ejection mechanism for neat PBT compared to the PA6:PBT blends, since ablation proceeds without the ejection of solid fragments.

3.6. Ablation craters

Fig. 8(a–l) present SEM images of the edges of the ablation craters obtained for all mixed compositions at fluences $F \simeq 2$ J cm^{-2} and $F \simeq 7$ J cm^{-2}. Moving from 1 wt% to 5 wt% PBT concentration, clear signs of fragmentation appear on the edge of the craters, as visible in Fig. 8(a–f) for both low and high fluence. Such fragments appear to be planar, indicating that they are part of a removed surface layer that is formed and detached from the bulk during the ablation process.

Fig. 8(g–l) show the morphology of the ablation craters obtained on PA6:PBT 80:20 and 60:40. Both at low and high laser fluence, some parallel stripes with a typical width of $\sim$ 20 μm are visible on the surface of the craters after irradiation. These stripes are formed by regions in which no ablation seems to have occurred, since no difference is visible between their surface morphology and that observed on the non-irradiated region outside the crater. This peculiar morphology will be discussed in detail in the following paragraph.

3.7. Ablation mechanism

The observed formation of detached surface layers as a consequence of the sea-island microstructure formed by PA6 and PBT and laser irradiation, is presented in Fig. 9(a–d), schematically illustrating the condition for low and high PBT concentration. The strongly optically absorbing PBT phase is surrounded by the transparent PA6 matrix, with a thickness depending on the composition of the blend (Fig. 2(f)). The incoming laser pulse is then absorbed in isolated regions containing PBT, where this polymer is rapidly heated up to sufficiently high temperatures to enable thermal vaporization and ionization. The heating process is also helped by the low heat conduction of the surrounding PA6 matrix, which does not allow energy dissipation through it, on a timescale comparable to the laser pulse duration. Additionally, both polymers have similar specific heats [22,23] and thermal decomposition temperatures in the interval between 400 °C and 500 °C [24–26], but PBT is thermally decomposed on a shorter timescale, due to the faster heating. The high-temperature decomposition products of PBT then exert pressure on the surrounding PA6 matrix while it is still mainly in the solid state, as confirmed by the fact that the holes left by PBT decomposition remain visible (see Fig. 10(a and b)). As a result, the thermal decomposition products of PBT remain confined inside the PA6 matrix, as a high-temperature ionized gas. This leads to the formation of localized high-pressure regions inside the domains initially occupied by PBT.

The formation of such high-pressure regions occurs at all PBT concentrations, since it is only due to the sea-island microstructure of the materials. However, a variation in the PBT concentration changes the number density of absorbing domains, as well as the distance between each other and from the surface of the film (Fig. 2(f)). This change in morphology affects the way the matrix breaks, following the formation of high-pressure regions, affecting impulse generation.

For PBT contents up to 5 wt%, the matrix fractures forming surface layers with typical length scale of $\sim$ 100 μm, as observed from SEM images of the surface of the craters in Fig. 8(a–f). The extension of these surface layers is sufficient to cover a large number of high-pressure PBT sites, as it appears clearly from Fig. 10(a and b). Consequently, before matrix breaking, high-pressure plasma produced by these sites cannot expand freely into vacuum because of the presence of the surface layer confining it.

For PBT concentrations of 20 wt% and 40 wt%, the morphology of ablation craters changes, showing the presence of surface PBT stripes alternated with regions that show matrix fragmentation (Fig. 11(a and b)). While laser ablation of PBT stripes leads to the ejection of only gaseous decomposition products, the ablation mechanism of the other regions proceeds similarly to how described for lower concentrations. The presence of a thinner matrix, however, does not allow the formation of large surface layers, so it breaks into smaller fragments, limiting the confinement effect.

Ablated mass and I_{sp} measurements support this description. For PBT concentrations higher than 1 wt%, I_{sp} appears to be roughly constant. This suggests that the ejection velocity v_e is not affected by the variations in microstructure caused by the different PBT content and that impulse generation is controlled by the amount of ejected mass. The observed maximum in impulse generation at 5 wt% is therefore due to an increased amount of mass that is accelerated at a similar ejection velocity obtained at other concentrations. Conversely, at higher PBT concentrations, a smaller amount of mass is accelerated roughly at the same velocity, despite the larger number of high-pressure sites formed below it. This suggests that the acceleration of the formed PA6 surface layers proceeds more efficiently in the 5 wt% case, reasonably due to the larger extension of the PA6 formed layers, which can more effectively confine the expanding gaseous ablation products.

The obtained spontaneous generation of a confinement layer was already observed in Ref. [15], where the same sea-island microstructure was obtained by using PLA as transparent matrix and PDoF containing reduced graphene oxide as absorbing phase. However in this study, the generation of a confinement layer is obtained by using different polymers and without other absorbers, indicating that the peculiar microstructure is the most important feature to enable this mechanism.

The different morphologies of the ablated craters at low and high ($\leq$ 20 wt%) PBT concentration can be attributed to composition-dependent changes in the melt rheology, which are not strictly linked to the ablation process. A change in the morphology of the craters is visible starting from the composition containing 20 wt% of PBT. In the compositions up to 5 wt% of PBT, the melt viscosity of the blend is

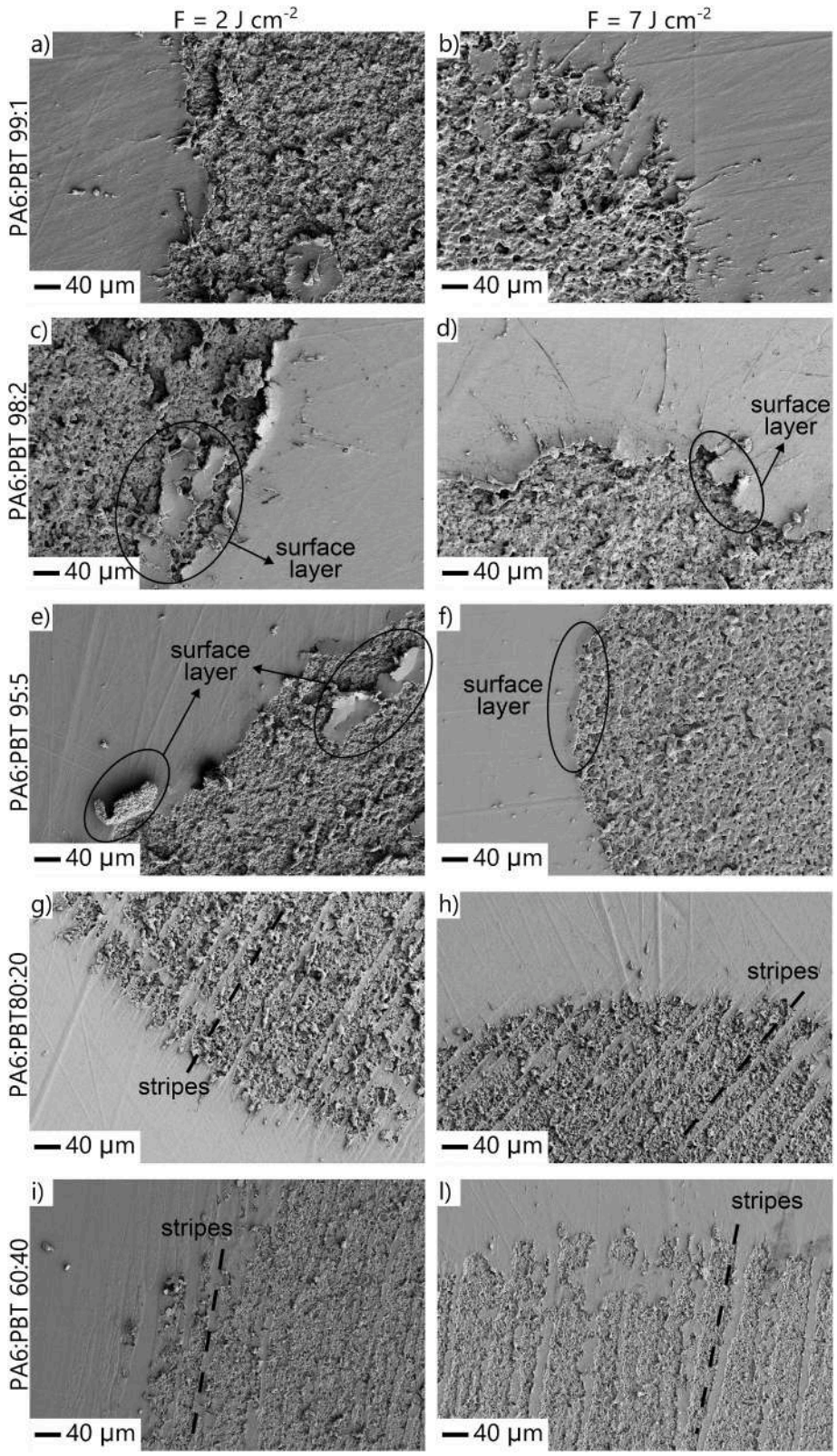

Fig. 8. SEM images of the edges of the ablation craters obtained after irradiation at 2 $J\ cm^{-2}$ and 7 $J\ cm^{-2}$.

dominated by PA6, as this is the most abundant phase. On the contrary, in the case of 20 and 40 wt% of PBT, the melt viscosity becomes strongly composition dependent, since the blend is closer to phase inversion. These compositional differences most likely strongly affect the melt behavior of the blends during the compression molding process [27–29].

Notably, even though the PBT domains appear spherical in the cross sections, as is visible in Fig. 2, the in-plane morphology on the top surface is markedly different. In the specific case, compression molding induces the in-plane stretching of PBT domains due to shear stress localized at the interfaces between domains-rich regions. Consequently,

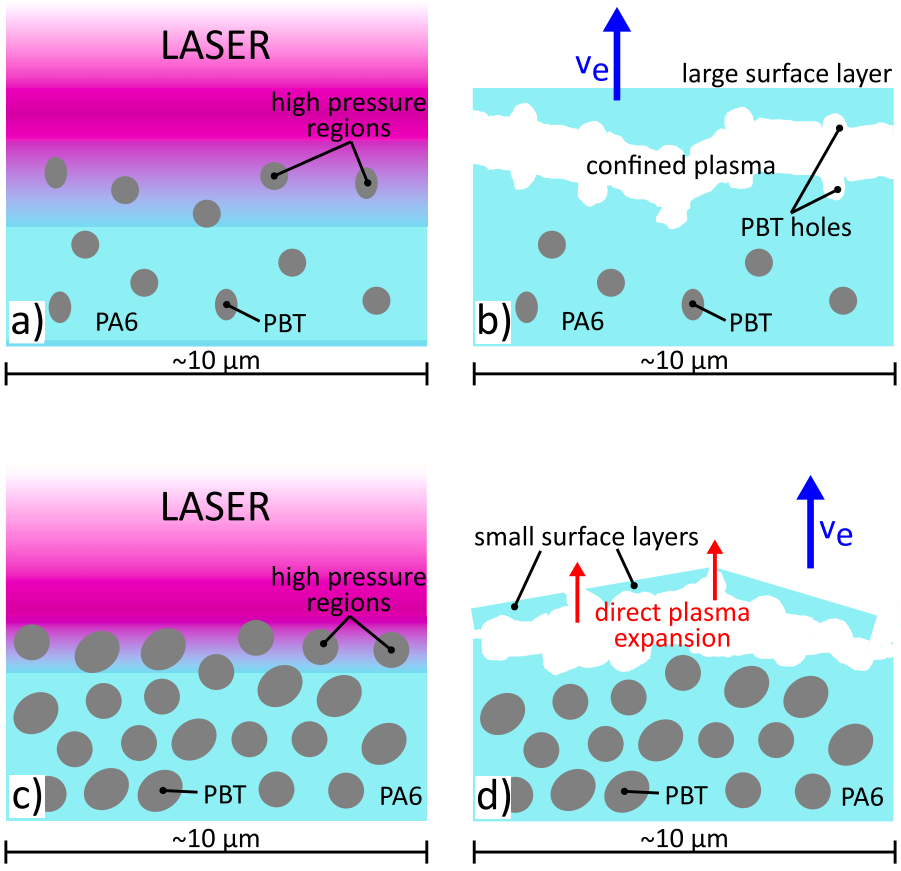

Fig. 9. Scheme of the generation of the surface layers. a), b) low PBT concentration (1,2,5 wt%), c), d) high PBT concentration (20,40 wt%) in the regions between the stripes.

radial melt channels that are visible on the top surface generate preferentially under heating and high pressure, and therefore freeze upon cooling, forming the visible stripes likely composed of PBT. In this context, laser ablation of the films enhances the contrast between the two immiscible phases, due to their different thermo-physical responses, but it is not directly involved in the formation of this peculiar morphology [30–32]. However, all hypotheses made relating to the shear-induced phase morphology changes still need some extent of validation, therefore, they will be properly investigated in future works by rheological and in-situ measurements.

The presented mechanism of spontaneous formation of a confinement layer obviously presents some differences compared to the classical case of confinement, where a transparent layer is positioned on top of an absorbing surface. In a typical confined geometry, a single, well-defined interface is present between the confinement layer and the absorbing surface. Additionally, the confinement layer is often considerably thick, of the order of ~ 100 μm [18] up to mm [16,17], becoming sufficiently resistant to avoid any rupture, being ejected as a single piece covering all the irradiated area. In some cases, these layers are also very massive, further increasing their capability of confining the underlying plasma plume. In such systems, therefore, very high C_m values of the order of $\sim 10^3$ μN/W can be generated, but with very low $I_{sp} \sim 1$ *s*. Considering, on the other hand, the sea-island microstructure here tested, it can be observed that many interfaces are present, located between the PBT domains and the transparent PA6 matrix surrounding them, and a proper comparison can only be done with our previous work [15]. However, laser absorption at these interfaces and the formation of localized high-pressure regions are observed to lead anyway to the formation of planar fragments, which act as confinement layers. Due to the non-uniform thickness of the matrix, the formed confinement layer is not as large as the irradiated area, but rather divided into many fragments that, as discussed, are sufficiently extended to hinder the expansion of the underlying plasma plume. Such a confinement mechanism is certainly less effective than the ideal case, however, it presents the outstanding property of being a consequence of the bulk structure of the target, and not of the presence of a bilayer geometry. Such a feature makes these kinds of materials promising for the development of advanced targets for LAP, capable of undergoing multiple irradiation cycles, while still delivering high impulse.

4. Conclusions

This work investigated the effects of the sea-island microstructure of targets obtained by mixing PA6 and PBT in laser ablation and in the consequent generation of a mechanical impulse.

PA6 and PBT were chosen because of their immiscibility and because of their different absorption coefficients, with PBT interacting more strongly with the present operating laser at a wavelength of 266 nm, as verified by UV-Vis spectroscopy.

Polymer blends in the form of films have been prepared by melt compounding and compression molding, using PBT as the minority phase, with concentrations ranging from 1 wt% to 40 wt%. SEM analysis

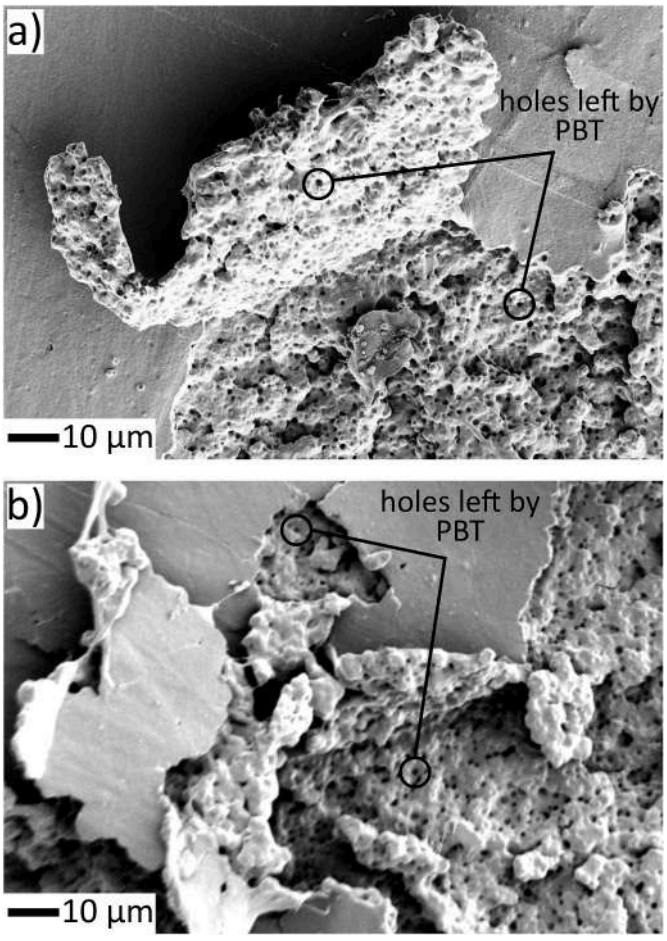

Fig. 10. SEM images of the edge of an ablation crater obtained at $F = 2\ J\ cm^{-2}$ on PA6:PBT 95:5, showing the detached layer and the holes left by PBT decomposition on both sides of the interface, confirming the mechanical fracture of the matrix. a) First laser pulse; b) third laser pulse.

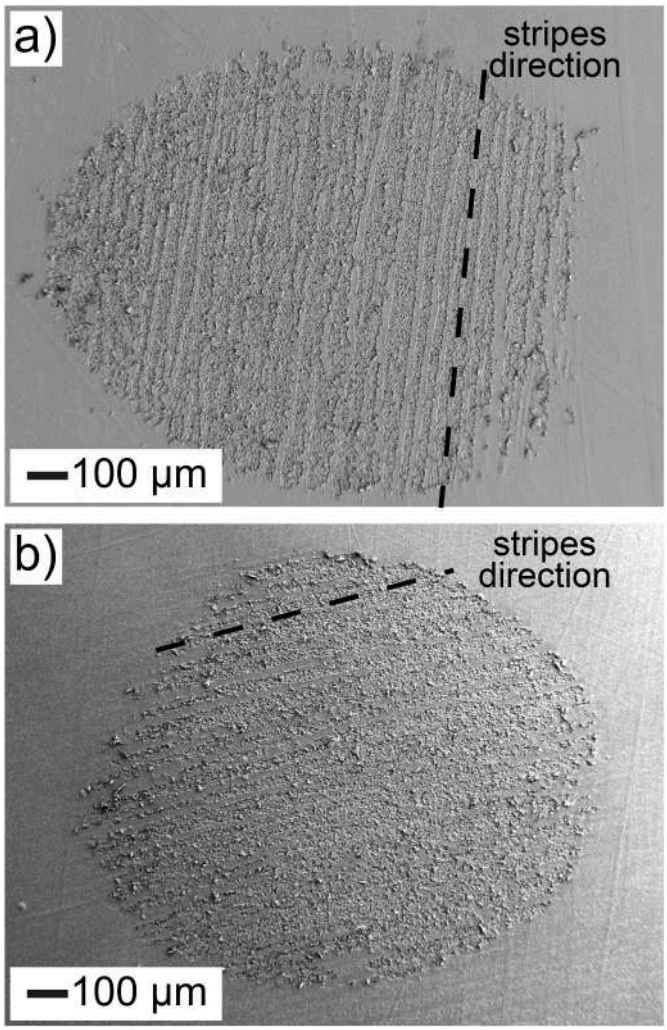

Fig. 11. Craters obtained on PA6:PBT 60:40 at $F \simeq 7\ J\ cm^{-2}$. a) And b) show a different orientation of the stripes obtained by rotating the target.

of the cross sections of the prepared films then revealed the formation of round PBT volumes with size and number density increasing with concentration, surrounded by a PA6 matrix.

Measurements of the impulse generated by laser ablation of the investigated materials were then conducted by irradiating the samples with laser fluences up to 7 J cm^{-2}, showing that the change in the microstructure induced by the different PBT concentrations affects impulse generation. Notably, it was observed that an increase in PBT content substantially reduces the fluence threshold for the generation of a mechanical impulse, reaching a value compatible with that of neat PBT for a concentration as high as 20 wt%. Moreover, for $F > 2$ J cm^{-2}, the impulse generation is maximized at 5 wt% PBT content, highlighting that the structure of the irradiated polymer is linked to the PBT content and plays a fundamental role in the ablation process. This result was shown to be related to an improved ablation efficiency of the blends, compared to PA6 and PBT.

The ablation mechanism was discussed by considering the evaluated mechanical impulse and performing SEM analysis on the ablation craters. The maximization of impulse observed for PA6:PBT 95:5 is likely related to the spontaneous formation of a confinement layer on the irradiated surface, due to the laser absorption at the interface between the PA6 matrix and the PBT domains. The absorbed laser radiation leads to the decomposition of the PBT domains into gaseous products, exerting pressure on the entire surrounding and overlying layer of material, leading to its fragmentation. In this regime, a larger amount of mass is accelerated more efficiently, leading to the improved impulse generation and C_m.

In case of higher PBT concentrations, the presence of aligned stripes of PBT on the ablated surface was observed. This is most probably related to the melt rheology of the blends, and it is not strictly associated with the laser ablation process. However, the presence of this heterogeneity of phases effectively impairs the ablation mechanism, showing no spontaneous confinement relevance, and consequently lower impulse values compared to 5 wt% of PBT.

Results obtained in this work show that the observed spontaneous formation of a confinement layer is a direct consequence of the sea-island microstructure obtained with immiscible polymers, when the more absorbing polymer is surrounded by the less absorbing one. Additionally, melt compounding and hot pressing proved to be effective for the synthesis of these materials, making the process more easily scalable. Obtained results also show that the impulse enhancement linked to confinement can also be maintained by irradiating the same region multiple times, leading to an attractive advantage from an application point of view.

CRediT authorship contribution statement

P. Battocchio: Writing – original draft, Visualization, Methodology, Investigation, Formal analysis, Data curation, Conceptualization. **D. Di Liberto:** Writing – original draft, Visualization, Methodology, Investigation, Formal analysis, Data curation, Conceptualization. **G. Fredi:**

Writing – review & editing, Methodology, Conceptualization. **A. Pegoretti:** Writing – review & editing, Supervision, Investigation. **A. Miotello:** Writing – review & editing, Supervision, Investigation.

Declaration of competing interests

The authors declare the following financial interests/personal relationships which may be considered as potential competing interests: Pietro Battocchio reports financial support was provided by Italian Space Agency and Ministero dell'Università e della Ricerca. Dalia Di Liberto reports financial support was provided by Italian Space Agency and Ministero dell'Università e della Ricerca. If there are other authors, they declare that they have no known competing financial interests or personal relationships that could have appeared to influence the work reported in this paper.

Acknowledgements

This study was carried out within the Space It Up project and received funding from the ASI and the MUR—Contract no. 2024-5-E.0-CUP no. I53D24000060005.

References

[1] A. Paravano, M. Patrizi, E. Razzano, G. Locatelli, F. Feliciani, P. Trucco, The impact of the new space economy on sustainability: an overview, Acta Astronaut. 222 (2024) 162–173, https://doi.org/10.1016/j.actaastro.2024.05.046.
[2] E.E. Areda, M. Hirokazu, M. Cho, Improving efficiency in CubeSat mass production: a modular and standardized approach, Acta Astronaut. 232 (2025) 51–67, https://doi.org/10.1016/j.actaastro.2025.02.017.
[3] V. Virendra Kumar, G. Rajan Kumar, P. Pramod Kumar, A re-examination of the space debris problem using systems thinking, Space Mission Planning & Operations 2 (1) (2023) 28–43, https://doi.org/10.20517/smpo.2022.05.
[4] C. Phipps, W. Bohn, T. Lippert, A. Sasoh, W. Schall, J. Sinko, A review of laser ablation propulsion, AIP Conf. Proc. (1) (2010) 710–722, https://doi.org/10.1063/1.3507164, 1278.
[5] Y. Nakamura, K. Kikuchi, G. Sekine, A. Isomura, A. Sasoh, S. Wada, K. Tsuno, T. Ogawa, T. Fukushima, Thrust performance of pulsed-laser ablation impulses for wavelengths of 1064 nm and 532 nm, Acta Astronaut. 232 (2025) 557–563, https://doi.org/10.1016/j.actaastro.2025.03.038.
[6] C.R. Phipps, M. Boustie, J.-M. Chevalier, S. Baton, E. Brambrink, L. Berthe, M. Schneider, L. Videau, S.A.E. Boyer, S. Scharring, Laser impulse coupling measurements at 400 fs and 80 ps using the LULI facility at 1057 nm wavelength, J. Appl. Phys. 122 (19) (2017), https://doi.org/10.1063/1.4997196.
[7] K. Suzuki, K. Sawada, R. Takaya, A. Sasoh, Ablative impulse characteristics of polyacetal with repetitive CO2 laser pulses, J. Propul. Power 24 (4) (2008) 834–841, https://doi.org/10.2514/1.32477.
[8] S. Rao, Y. Xu, J. Yuan, F. Liu, S. Wang, H. Jiang, G.J. Cheng, MOFs for ultrahigh efficiency pulsed laser micropropulsion, Adv. Mater. 36 (1) (2024) 2306228, https://doi.org/10.1002/adma.202306228.
[9] P. Battocchio, N. Bazzanella, M. Orlandi, G. Ischia, A. Miotello, Carbon nanoparticles as absorbers in PVC for laser ablation propulsion: size effects, Appl. Phys. A 129 (3) (2023) 220, https://doi.org/10.1007/s00339-023-06502-7.
[10] P. Battocchio, J. Terragni, V. Cristino, N. Bazzanella, R. Checchetto, M. Orlandi, S. Caramori, A. Miotello, Poly(vinyl chloride) coupling with UV laser radiation: Comparison between polymer absorbers and nanoparticles to increase efficiency for laser ablation propulsion, J. Phys. Chem. C 125 (51) (2021) 28088–28099, https://doi.org/10.1021/acs.jpcc.1c08175.
[11] L. Urech, T. Lippert, C.R. Phipps, A. Wokaun, Polymers as fuel for laser-based microthrusters: an investigation of thrust, material, plasma and shockwave properties, Appl. Surf. Sci. 253 (19) (2007) 7646–7650, https://doi.org/10.1016/j.apsusc.2007.02.032.
[12] Y. Ou, J. Wu, Y. Zhang, J. Li, Y. Zhao, Plume characteristics of polymeric material doped with different metal particles under pulsed laser irradiation, Opt Laser. Technol. 152 (2022) 108132, https://doi.org/10.1016/j.optlastec.2022.108132.
[13] Z. Ma, Y. Ou, J. Wu, X. Liu, Unveiling the ablation mitigation mechanism of metal mesh reinforced polytetrafluoroethylene composites under repetitive pulsed laser irradiation, Acta Astronaut. 245 (2026) 179–193, https://doi.org/10.1016/j.actaastro.2026.02.045.
[14] S. Wang, B. Du, B. Xing, Y. Hong, Y. Wang, B. Du, Y. Zheng, J. Ye, C. Li, Interface Adhesion Property and Laser Ablation Performance of GAP-PET Double-Layer Tape with Plasma Treatment, vol. 12, 2022, p. 1827, 11.
[15] P. Battocchio, G. Fredi, N. Bazzanella, R. Checchetto, D.N. Bikiaris, D. Maniglio, A. Pegoretti, A. Miotello, Improved laser ablation propulsion efficiency in composite polymers, containing reduced graphene oxide, by the spontaneous formation of a confining layer, Appl. Surf. Sci. 687 (2025) 162251, https://doi.org/10.1016/j.apsusc.2024.162251.
[16] C. Le Bras, E. Lescoute, J.-M. Chevalier, G. Boutoux, D. Hébert, Impulse coupling enhancement of aluminum targets under laser irradiation in a soft polymer confined geometry, J. Appl. Phys. 136 (11) (2024), https://doi.org/10.1063/5.0225973.
[17] R. Fabbro, J. Fournier, P. Ballard, D. Devaux, J. Virmont, Physical study of laser-produced plasma in confined geometry, J. Appl. Phys. 68 (2) (1990) 775–784, https://doi.org/10.1063/1.346783.
[18] S. Ly, J. Lee, A.M. Rubenchik, J.C. Crowhurst, C.D. Boley, V.N. Peters, W.J. Keller, Tamper performance for confined laser drive applications, Opt. Express 31 (14) (2023) 22532–22553, https://doi.org/10.1364/oe.491526.
[19] P. Battocchio, M. Bembli, N. Bazzanella, M. Biesuz, M. Scarpa, G.D. Sorarù, A. Miotello, Laser propulsion in confinement regime: the role of film thickness in the impulse generation process, Appl. Sci. 16 (1) (2026) 224, https://doi.org/10.3390/app16010224.
[20] P. Battocchio, J. Terragni, N. Bazzanella, C. Cestari, M. Orlandi, W.J. Burger, R. Battiston, A. Miotello, Ballistic measurements of laser ablation generated impulse, Meas. Sci. Technol. 32 (1) (2021) 015901, https://doi.org/10.1088/1361-6501/abace6.
[21] K. Suzuki, K. Sawada, R. Takaya, A. Sasoh, Ablative impulse characteristics of polyacetal with repetitive CO2 laser pulses 24 (4) (2008) 834–841, https://doi.org/10.2514/1.32477.
[22] C. Millot, L.-A. Fillot, O. Lame, P. Sotta, R. Seguela, Assessment of polyamide-6 crystallinity by DSC, J. Therm. Anal. Calorim. 122 (1) (2015) 307–314, https://doi.org/10.1007/s10973-015-4670-5.
[23] M. Pyda, E. Nowak-Pyda, J. Mays, B. Wunderlich, Heat capacity of poly(butylene terephthalate), J. Polym. Sci. B Polym. Phys. 42 (23) (2004) 4401–4411, https://doi.org/10.1002/polb.20286.
[24] F. Samyn, S. Bourbigot, Thermal decomposition of flame retarded formulations PA6/aluminum phosphinate/melamine polyphosphate/organomodified clay: interactions between the constituents? Polym. Degrad. Stabil. 97 (11) (2012) 2217–2230, https://doi.org/10.1016/j.polymdegradstab.2012.08.004.
[25] M. Herrera, G. Matuschek, A. Kettrup, Main products and kinetics of the thermal degradation of polyamides, Chemosphere 42 (5) (2001) 601–607, https://doi.org/10.1016/S0045-6535(00)00233-2.
[26] G. Montaudo, C. Puglisi, F. Samperi, Primary thermal degradation mechanisms of PET and PBT, Polym. Degrad. Stabil. 42 (1) (1993) 13–28, https://doi.org/10.1016/0141-3910(93)90021-A.
[27] T. Ougizawa, T. Inoue, Morphology of Polymer Blends in *Polymer Blends Handbook*, Springer Netherlands, Dordrecht, 2014, pp. 875–918, https://doi.org/10.1007/978-94-007-6064-6_10.
[28] P. Van Puyvelde, A. Vananroye, R. Cardinaels, P. Moldenaers, Review on morphology development of immiscible blends in confined shear flow, Polymer 49 (25) (2008) 5363–5372, https://doi.org/10.1016/j.polymer.2008.08.055.
[29] I. Otero Navas, M. Kamkar, M. Arjmand, U. Sundararaj, Morphology evolution, molecular simulation, electrical properties, and rheology of carbon nanotube/polypropylene/polystyrene blend nanocomposites: effect of molecular interaction between styrene-butadiene block copolymer and carbon nanotube, Polymers 13 (2) (2021), https://doi.org/10.3390/polym13020230.
[30] N. Arjomand, M. Mohamadi, J.A. Kaklar, Development of a morphological-based predictive model for mechanical properties of binary immiscible polymer blends considering interfacial effects, Sci. Rep. 15 (1) (2025) 7177, https://doi.org/10.1038/s41598-025-90421-5.
[31] R. Banerjee, S.S. Ray, Role of rheology in morphology development and advanced processing of thermoplastic polymer materials: a review, ACS Omega 8 (31) (2023) 27969–28001, https://doi.org/10.1021/acsomega.3c03310.
[32] G. Verfaillie, J. Devaux, R. Legras, Relationship between surface and bulk morphologies for immiscible polymer blends, Polymer 40 (11) (1999) 2929–2938, https://doi.org/10.1016/S0032-3861(98)00336-X.